Chinese Chemical Letters 34 (2023) 107793

Contents lists available at ScienceDirect

Chinese Chemical Letters

journal homepage: www.elsevier.com/locate/cclet

Surface engineering for high stable lithium-rich manganese-based cathode materials

Miaomiao Zhou[a,1], Jianjun Zhao[b,1], Xiaodong Wang[a,1], Ji Shen[c], Wenhao Tang[a], Yirui Deng[a], Ruiping Liu[a,c,*]

[a] School of Chemical & Environmental Engineering, China University of Mining and Technology (Beijing), Beijing 100083, China
[b] State Key Laboratory of Chemical Resources Engineering, Beijing Advanced Innovation Center for Soft Matter Science and Engineering, College of Chemistry, Beijing University of Chemical Technology, Beijing 100029, China
[c] Department of Materials Science and Engineering, China University of Mining & Technology (Beijing), Beijing 100083, China

ARTICLE INFO

Article history:
Received 16 June 2022
Revised 10 July 2022
Accepted 12 August 2022
Available online 2 September 2022

Keywords:
Li-rich layered oxide
Li-ion batteries
$La(PO_3)_3$ coating
Electrochemical performance
Structure stability

ABSTRACT

Lithium-rich manganese-based material shows great potential as the high specific cathode materials due to its low cost, environmental friendliness, high operating voltage and simple preparation process. However, the poor capacity retention and cycling performance caused by its unstable structure during cycling restrict the commercialization. In this work, $Li_{1.2}Ni_{0.16}Mn_{0.56}Co_{0.08}O_2$ was synthesized utilizing a Co-precipitation method and different amount of $La(PO_3)_3$ ($La(PO_3)_3 = 2$ wt%, 4 wt% and 6 wt%) was selected as the coating layer to resolve the above issues. During the calcination process, $La(PO_3)_3$ reacts with impurities such as LiOH and Li_2CO_3 on the lithium-rich surface to reduce the residual lithium on the surface, thus improving the interfacial stability, slowing down the corrosion of the electrolyte, and finally enhancing its electrochemical performance. The cathode materials coated with 4% of $La(PO_3)_3$ showed the best electrochemical performance in terms of capacity retention and cycling performance compared to the pristine NCM. The high initial discharge capacity of 214.21 mAh/g and capacity retention of 94.2% after 100 cycles at 0.1 C can be obtained. This work provides an effective strategy to protect the cathode from corrosion and will promote its further practical applications in high specific Li-ion batteries.

Against the backdrop of serious environmental problems caused by the increasing consumption of fossil fuels, lithium-ion batteries, act as a clean energy source used in portable electronic devices, have become an indispensable part of human life [1–3]. As the energy density of lithium-ion batteries is partially determined by the cathode [4,5], and traditional cathode materials such as $LiCoO_2$ and $LiFePO_4$ cannot meet the ever growing requirement of energy density with the increasing demand for portable energy storage devices, long-haul electrical vehicles (EV) and hybrid electrical vehicles (HEV), it is crucial to develop cathode materials with high-capacity and high voltage [6–8].

Recently, lithium-rich manganese-based cathode materials ($xLi_2MnO_3(1\text{-}x)LiMO_2$ (M = Mn, Ni, Co)) has attracted a lot of concern from scientists, due to the high charging voltage, a theoretical specific capacity of 250 mAh/g, and high energy density (1000 Wh/kg) [9–11]. At the same time, these materials also have many other advantages, such as good crystallinity, abundance and environmental friendliness of Mn [12–15]. However, the low initial coulombic efficiency, severe voltage capacity fade during cycling, and poor rate behavior limit the practical application of Li-rich cathode materials to some extent [16–18]. Moreover, during the preparation process, part of the lithium ions will enter the lattice to form a stable structure, and many residual Li^+ in the form of Li_2O will react with the water and oxygen wrapped around the surface of the cathode material to form residual lithium compounds such as Li_2CO_3 or LiOH [19–21], which will damage the surface structure, causing the increase of the irreversible capacity and reduction of the transfer-transport coefficient of lithium ions, and finally severely hindering the electrochemical performance of lithium-rich cathodes [22–25].

Surface coatings have been considered as an effective way to improve the cycling stability and rate capability of cathode materials [26]. The surface coating has been proven to protect the active material from corrosion by hydrofluoric acid by avoiding direct contact with the electrolyte, preserving the oxygen ion vacan-

* Corresponding author at: School of Chemical & Environmental Engineering, China University of Mining and Technology (Beijing), Beijing 100083, China.
E-mail address: lrp@cumtb.edu.cn (R. Liu).
[1] These authors contributed equally to this work.

https://doi.org/10.1016/j.cclet.2022.107793
1001-8417/

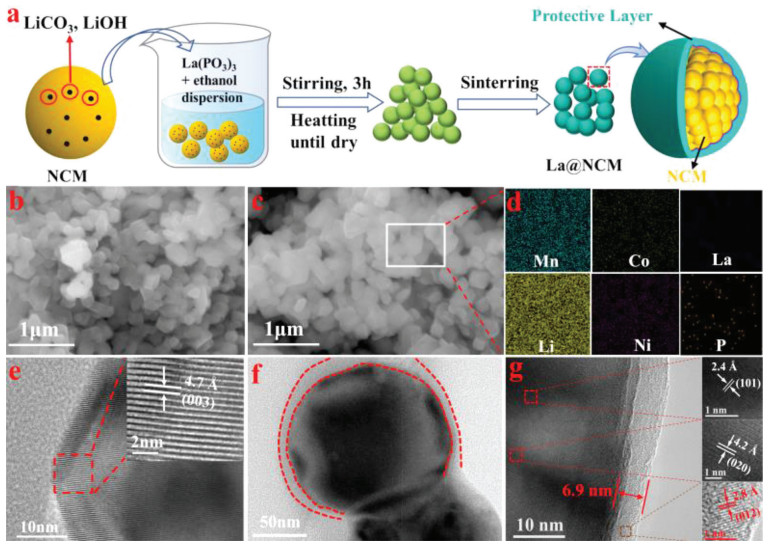

Fig. 1. (a) Schematic illustration of the preparation process. SEM images of (b) NCM and (c) 4% La@NCM, (d) EDS spectra of 4% La@NCM. TEM images of (e) NCM, (f, g) 4% La@NCM.

cies, reducing the oxygen ion activity and inhibiting oxygen loss [27–29]. Surface modifications with metal oxides [30], fluorides [31] and carbon [32] materials are commonly used to stabilize the interfacial structure and mitigate electrolyte corrosion of lithium-rich cathode materials. A thin layer of Al_2O_3 on the surface of the cathode material could improve its electrochemical performance and stability [33,34]. ZnO coating can reduce the side reaction between electrolyte and cathode and stabilize the surface structure of electrode [35]. The initial irreversible capacity of the cathode material can be reduced by coating a certain amount of MoO_3 [36,37], However, the lower conductivity of metal oxide will increase the transmission path of lithium ions [38]. The cathode material after coating with fluoride is less prone to phase change at high temperature and has high thermal stability, the fluoride coating will increase the irreversible capacity and reduce the initial Coulomb efficiency [39], and carbon layer shows little improvement to the electrochemical performance [40,41].

Metaphosphate is a three-dimensional lattice-like crystal, and it can react with alkaline materials under sintering conditions to form a complex phosphate. Furthermore, due to its polyanionic characteristic, the binding of oxygen by the polyanionic group may reduce the oxygen release from the cathode material [42–44], which can improve the thermal and structural stability and cycling performance of the lithium-rich manganese-based cathode materials when employed as a protective layer. Herein, the lithium-rich manganese-based cathode materials ($Li_{1.2}Ni_{0.16}Mn_{0.56}Co_{0.08}O_2$) were synthesized by co-precipitation method, and a three-dimensional lattice-like crystalline $La(PO_3)_3$ was selected as the coating material, which is a polyanionic material that can neutralize and react with Li_2CO_3 and LiOH on the surface of Li-rich materials under the suitable sintering temperature to generate metal phosphate compounds. This reduces the residual lithium on the surface of the cathode material, improves the rate performance and slows down the corrosion of HF corrosion. Meanwhile, a small amount of La will enter the cathode materials during the sintering process to prevent Ni/Li from mixing, and thus stabilizing the structure and improving the cycling performance of the lithium-rich cathode materials.

The schematic diagram showing the preparation and mechanism of the lithium-rich manganese-based cathode material is illustrated in Fig. 1a. $Li_{1.2}Ni_{i0.16}Mn_{0.56}Co_{0.08}O_2$ (NCM) was prepared by using co-precipitation method firstly, weigh the appropriate amount of $La(PO_3)_3$ into the beaker with ethanol ultrasonically dispersed, add the obtained NCM slowly to the solution, stir for 3 h, and then the modified cathode material, namely La@NCM, was obtained under suitable sintering conditions. The morphology and EDS analysis of the as-prepared smples were investigated by SEM (Figs. 1b and c, Figs. S1a-d in Supporting information). The SEM morphologies of all samples are not very different, and the particle size does not change abruptly after coating, which is about 100–150 nm. Fig. 1d shows the elemental distribution of 4% La@NCM, it can be seen that Li, Ni, Mn and Co are uniformly distributed on the surface of the material, and La and P elements are also detected, indicating the successful $La(PO_3)_3$ coating formation.

TEM and HRTEM were employed to get further insights into the structural characteristics of the hybrid coating layer (Figs. 1e-g). The lattice stripe spacing of pristine NCM is 0.47 nm, which is consistent with the distance of the (003) crystal plane, revealing its well-developed laminar structure (Fig. 1e). A well-defined layer on the surface of the 2% La@NCM can be found (Fig. S2 in Supporting information). Figs. 1f and g reveal that a thin layer with the thickness of about 6.9 nm that uniformly covers the surface of the 4% La@NCM particles, and the stripe spacing of 0.24 nm and 0.42 nm correspond to the (101) plane of the lamellar structure and (020) crystal plane of monoclinic Li_2MnO_3, respectively, confirming the existence of both the lamellar structure and spinel structure. Meanwhile, it is shown in Fig. 1g that there are some local lattice fringes in the coating, and the spacing of the lattice fringes is about 0.28 Å, corresponding to the (012) crystal plane of $LaPO_4$, indicating that $LaPO_4$ is well crystallized. The sintering temperature affects the formation and crystallinity of phosphate to a certain extent, which is manifested as the formation of local lattice fringe of $La(PO_3)_3$ in the coating. A heterogeneous and unbounded thick coating layer on the surface of the 6% La@NCM particles can be observed, and the magnification image further demonstrates that it has an irregular morphology, indicating an excess of coating (Figs. S3a and b in Supporting information). The surface area of pristine NCM is 4.2681 m^2/g, and the specific surface area of 4% La@NCM and 6% La@NCM is 4.2880 m^2/g and 4.0720 m^2/g, respectively (Fig. S4 in Supporting information). The specific surface area is reduced when incorporating a large amount of $La(PO_3)_3$ coating materials. The particles will agglomerate when increasing the amount of coating material, and it can be inferred that the active atoms located in the center of the NCM are unable to participate in the electrochemical reaction and cannot fully exert the discharge per-

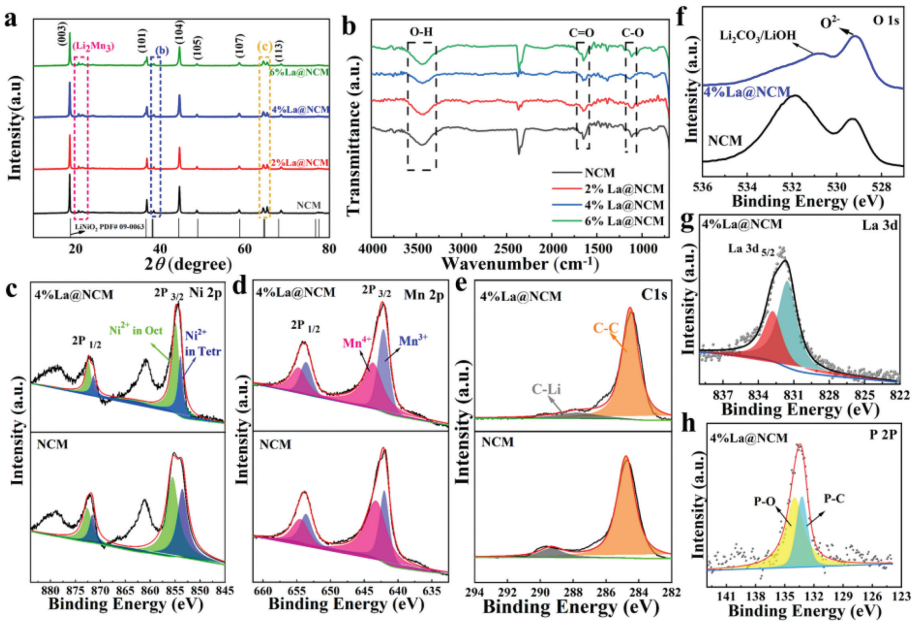

Fig. 2. (a) XRD patterns and (b) FTIR spectra of NCM, 2% La@NCM, 4% La@NCM, 6% La@NCM. XPS spectra of (c) Ni 2p, (d), Mn 2p, (e) C 1s and (f) O 1s of the NCM and 4% La@NCM. XPS spectra of (g) La 3d and (h) P 2p of 4% La@NCM.

formance duration the charging and discharging cycle, resulting in the loss of capacity.

Figs. 2a and b and Fig. S5 (Supporting information) display the XRD patterns and the FTIR spectra of samples. All samples show almost the same diffraction peaks with the hexagona α-$NaFeO_2$ phase (R-3m). Meanwhile, the lithium-rich characteristic peak of Li_2MnO_3 with monoclinic crystal structure can be observed at 2θ of 20°−23°. The two groups of two split peaks (006)/(102) and (108)/(110) can also be clearly observed, which are enlarged in (Fig. S5), and the obvious splitting confirms that all samples maintain a high crystallinity. The crystallite parameters of the four groups of samples are shown in Table S1. It can be concluded that the c/a values of all the four samples are greater than 4.9, which further indicates the well-structured characteristics of the samples. The I_{003}/I_{104} values of La@NCM are smaller than those of NCM, which can be ascribed to that the polyanion $La(PO_3)_3$ can promote the formation of spinel phase. Among them, 4% La@NCM shows the least Ni-Li mixing and larger lattice spacing, which will be beneficial to Li^+ transport and finally helpful to enhance the rate performance of the materials. Combined with Fig. S6 (Supporting information), it can be concluded that the existence of coating layer can improve the thermal stability of lithium-rich manganese-based cathode materials. The enhanced thermal stability of 4% La@NCM was ascribed to the formed spinel phase [45], which not only effectively restrained the oxygen evolution during the electrochemical process, but also acted as the stable protective layer, stabilizing the interface structure, and inhibiting the side reaction between the cathode and electrolyte.

FTIR tests were used to clarify the interfacial states of the samples and the influence of moisture was strictly controlled throughout the test process, as shown in Fig. 2b. The absorption peaks at 1100 cm^{-1} and 1600 cm^{-1} are assigned to C=O stretching vibration and C-O stretching mode, respectively, which are due to the formation of Li_2CO_3 by the reaction between the residual lithium on the surface of the cathode material and water and carbon dioxide in the air. The absorption peak near 3400 cm^{-1} can be attributed to the O-H of LiOH. The intensity of the C-O, C=O and O-H functional groups decreases and then increases with the increase of $La(PO_3)_3$ content. The 4% La@NCM shows the lowest intensity, indicating that the appropriate amount of coating can alleviate the formation of LiOH and Li_2CO_3. The formed Li_2CO_3 will affect the de-embedding of Li^+, destroy the structure of the surface, and deteriorate the electrochemical properties of the cathode materials.

X-ray photoelectron spectroscopy (XPS) was used to analyze the valence state of cathode materials before and after coating as shown in Figs. 2c-h and Fig. S7 (Supporting information). In Fig. 2c, two sets of peaks at 872.9 eV and 856.3 eV can be assigned to Ni $2p_{3/2}$ and Ni $2p_{1/2}$, respectively, implying the presence of Ni^{2+} in the cathode materials. The smaller area of Ni^{2+} at Ni $2p_{1/2}$ for the 4% La@NCM indicates that fewer Ni^{2+} ions in the Tm layer enters the Li layer and the reduced Li/Tm mixing, which is consistent with the previous XRD results [46,47]. The main peaks located at 642.6 eV and 654.2 eV belong to Mn $2p_{3/2}$ and Mn $2p_{1/2}$, respectively (Fig. 2d). The increase of Mn^{3+} after coating with 4% of $La(PO_3)_3$ is consistent with the previously reported results. It indicates that a small amount of La elements infiltrated into the NCM and excited more active Mn^{3+} during coating process. The characteristic peaks of Co elements at around 780 eV and 795 eV are mainly in the form of +3 valence, which is also consistent with the results of the NCM materials (Fig. S8 in Supporting information). Fig. 2e shows the C1s profiles of the two groups of materials, and the peaks at 289.3 eV and 285.1 eV correspond to the C-Li and C-C bonds, respectively. After coating with 4% of $La(PO_3)_3$, the area of C-Li bond is reduced, which indicates that the formation of Li_2CO_3 on the particle surface is reduced. The O1s profiles of the two groups of materials show that the characteristic peaks of Li_2CO_3 and LiOH at 532 eV almost disappear, while the characteristic peak of O^{2-} at 529.2 eV remains unchanged, indicating that the residual lithium on the cathode material surface can be effectively reduced by coating with $La(PO_3)_3$ layer (Fig. 2f). The La and P elements are also detected in the coated NCM, the valence state of La is attributed to $LaPO_4$, and the spectrum of P is at 129–139 eV, which confirms the presence of the mixture of $(PO_3)^{3-}$ and $(PO_4)^{3-}$ in Figs. 2g and h. The coating can reduce the direct contact area between the bulk phase material and electrolyte, slow down the direct side reactions and improve the electrochemical performance of lithium-rich materials.

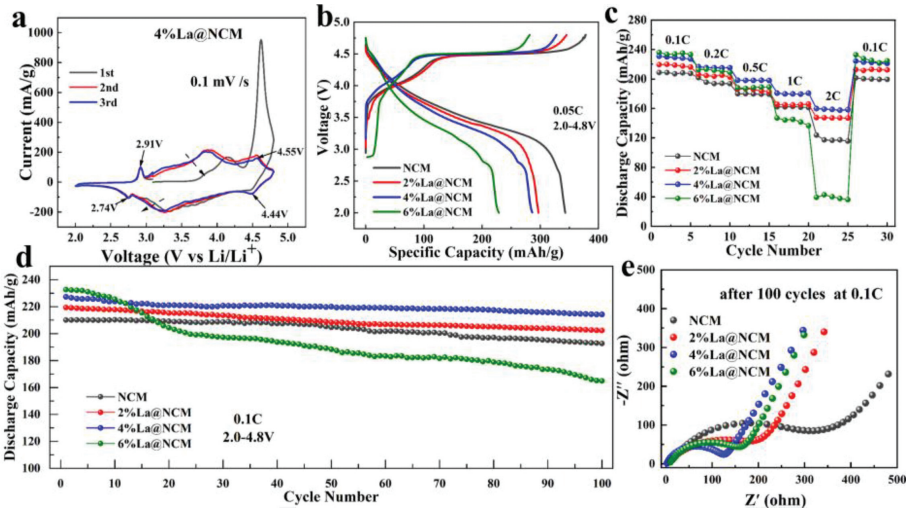

Fig. 3. (a) CV curves of the 4% La@NCM. (b) The initial discharge-charge curves, (c) The rate performance and (d) cycling performance of the cells. (e) Nyquist plots of samples after one hundred cycles.

The cyclic voltammetric curves were tested to elaborate the electrochemical mechanisms of the cathode materials during cycling, as shown in Fig. 3a and Figs. S9a-c (Supporting information). The oxidation peak at 4.0 V can be ascribed to the oxidation of Ni^{2+} to Ni^{4+} and Co^{3+} to Co^{4+} in $LiMO_2$ (M = Mn, Ni, Co) and the irreversible oxidation peaks at 4.6 V is assigned to the detachment of Li_2O from Li_2MnO_3 to form MnO_2. For the NCM materials without coating, the oxidation peak at 4.6 V is sharp and obvious during the first scan, while the intensity of the peak gradually decreases and even disappears during the second to fifth scan. After coating with $La(PO_3)_3$, the existence of the oxidation peak at 4.6 V during cycling indicates that the $La(PO_3)_3$ coating can constantly activate the layered structure in the structure. The reduction peak of pristine NCM at 3.2 V during the negative sweep is due to the reduction of Mn^{4+} to Mn^{3+}, while after coating with 4% $La(PO_3)_3$, the reduction peak at 3.2 V can only be found after the full activation by Li_2MnO_3 in the fourth and fifth scans, which indicates that the appropriate amount of $La(PO_3)_3$ coating will reduce the oxygen loss in the material. In addition to the redox peaks mentioned above, a new oxidation peak appears in CV curves of 2% La@NCM, 4% La@NCM and 6% La@NCM at about 2.7–2.9 V, which is related to the formation of the spinel structure and corresponds to the short plateau of 2.75 V in the first discharge curve of 2% La@NCM, 4% La@NCM and 6% La@NCM [48,49]. The electrode materials with coating layer has a high degree of overlap in the fourth and fifth CV cycles, indicating its good cyclic reversible performance.

To investigate the electrochemical performance of the cathode materials, the cells with different cathode materials were cycled at 2.0–4.8 V. The first charge/discharge curves of NCM, 2% La@NCM, 4% La@NCM, and 6% La@NCM show no significant difference with the increases of the amount of $La(PO_3)_3$ coating. The initial discharge specific capacities of NCM, 2% La@NCM, 4% La@NCM and 6% La@NCM at 0.05 C are 342.91 mAh/g, 296.83 mAh/g, 286.15 mAh/g and 228.81 mAh/g, respectively (Fig. 3b). The pristine NCM has the highest discharge specific capacity at the initial cycle, and the samples with coating layer show reduced lithium storage capacity due to the lower activity of the coating materials. The 6% La@NCM has the smallest primary discharge capacity due to the thick and uneven coating layer, which results in the transportation difficulty of lithium ions (Fig. 3b). The rate performance of the NCM cathode material is greatly improved by coating 4% $La(PO_3)_3$, and the discharge capacity of 227.11 mAh/g, 215.21 mAh/g, 198.02 mAh/g, 180.76 mAh/g and 158.40 mAh/g can be obtained at 0.1 C, 0.2 C, 0.5 C, 1 C and 2 C, respectively (Fig. 3c). More significantly, a high discharge capacity of 221.07 mAh/g is recovered after the current density returns to 0.1 C, indicating that the material has good rate behavior. The appropriate amount of $La(PO_3)_3$ coating can neutralize the residual lithium salt on the surface of the lithium-rich material and form the new compound, which will improve the ionic conductivity of the material and thus enhance the rate performance. The discharge specific capacities after 100 cycles of NCM, 2% La@NCM, 4% La@NCM and 6% La@NCM at 0.1 C are 192.70 mAh/g, 202.36 mAh/g, 214.21 mAh/g and 164.98 mAh/g, and the capacity retention rates are 91.7%, 92.2%, 94.2%, and 70.9%, respectively. In order to explore the electrochemical performance of the coating material at high rate, the cycle test of the four samples have been carried out at 1 C rate (1 C = 230 mAh/g), as shown in the Fig. S10 (Supporting information). The discharge specific capacities after 50 cycles of NCM, 2% La@NCM, 4% La@NCM and 6% La@NCM at 1 C are 141.73 mAh/g, 153.38 mAh/g, 170.40 mAh/g and 98.38 mAh/g, and the capacity retention rates are 85.7%, 87.6%, 92.5%, 69.9%, respectively. When the current increases, the samples with more coating decays more rapidly, and the discharge specific capacity is the lowest. The capacity of the pristine sample NCM is slightly lower, and the high rate and cycling performance of 4% La@NCM are the best, which is consistent with the cycle at low current. With increasing the $La(PO_3)_3$ coating amount, the discharge capacity of cathode materials increases firstly and then decreases, and the highest capacity retention of 94.2% can be obtained with 4% of $La(PO_3)_3$ coating (Fig. 3d). The thinner/thicker and uneven coating layer will inevitably cause the capacity reduction. It further indicates that the protective layer formed by the reaction between appropriate amount of $La(PO_3)_3$ and the residual lithium salt on the surface of the lithium-rich material can alleviate the corrosion of the cathode material caused by the electrolyte during the cycling process.

Fig. 3e and Fig. S9d (Supporting information) show the Nyquist plots of all the samples. The semicircle in the high frequency region reflects the charge transfer resistance (R_{ct}), and the R_{ct} value increases slightly with increasing the coating material (Table S2 in Supporting information). The R_{ct} values of NCM, 2% La@NCM, 4% La@NCM and 6% La@NCM are 39.74 Ω, 45.92 Ω, 47.84 Ω and 58.01 Ω, respectively; after 100 cycles at 0.1 C, the R_{ct} values are 231.8 Ω, 197.7 Ω, 122.1 Ω, and 149.6 Ω, respectively. It can be noted that the NCM sample has the largest R_{ct} value, while 4% La@NCM exhibits the smallest R_{ct} value after cycling. Before cy-

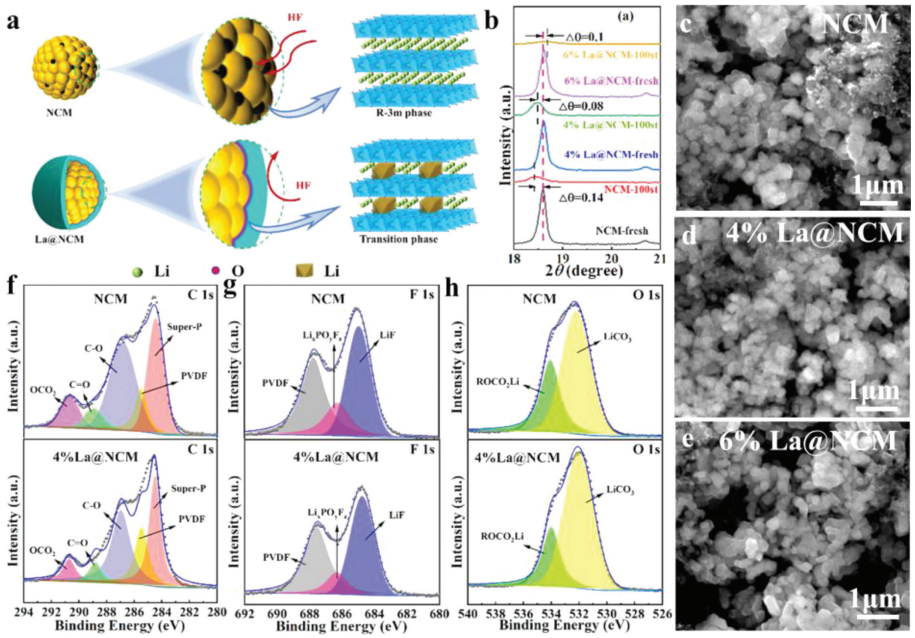

Fig. 4. (a) Schematic diagram of surface modified NCM. (b) XRD patterns of magnified diffraction peaks of (003) and (c-e) SEM images of NCM with different amount of La after 100 cycles. (f) C 1s spectra, (g) F 1s spectra, (h) O 1s spectra of NCM and 4%La@NCM electrodes after 100 cycles.

cling, the wrapped phosphate on the surface of the material hinders the movement of metal ions, the pristine NCM cathode materials suffer from electrolyte corrosion during cycling, while the moderate amount of $La(PO_3)_3$ coating alleviates the corrosion of HF on the surface of the particles and the structure of the cathode material was stabilized, resulting in a lower R_{ct} value.

To probe the effect of the coating layer on the electrode during the charging and discharging process, XRD patterns, the morphologies, and XPS of the cathode materials after 100 cycles were observed. Fig. 4a show in the process of calcination that metal complex phosphate layer on the surface of cathode materials can be formed, which plays the role of solid glass electrolyte with high temperature resistance and fire resistance oxygen suppression, and the coating formation can effectively resist the side reaction between the electrode material and HF. The surface layer of the pristine NCM particles is R-3m layered structure, while the modified material will form a uniform protective film on the surface of the particles, and in the area where the particles are in contact with the protective layer, the crystal structure belongs to the spinel structure, which will induce a few Ni^{2+} ions into the Li layer, causing the Ni-Li mixing in some areas. Furthermore, the spinel structure is more stable than the lamellar structure, which hinders the O^{2-} transportation, thus reducing the oxygen loss in the material and stabilizing the crystal structure of Li-rich Mn-based cathode material during cycling.

As shown in Fig. S11 (Supporting information), the XRD patterns of the recovered samples provide evidence of the quantitative phase change of the material. After cycling, all samples remain the same lamellar structure with different degrees of diffraction intensity reduction of the main (003) peak, which means that the material was also damaged to different degrees during cycling. The large fluctuations of the pristine NCM (003) peak represent the contraction in the a and b axes and coexisting lattice extension in the c axis, while the smallest deviation of the (003) peak position for the 4% La@NCM sample indicates the 4% La@NCM sample showed that the appropriate amount of cladding suppressed the phase change of the material to some extent that implying that the material is structurally intact with minimal damage after cycling (Fig. 4b).

Fig. 4c shows that the NCM pole pieces fall off more seriously, while after cycling, the surface of the particles without coating is severely corroded by the electrolyte. The particles with 4% of $La(PO_3)_3$ coating remain intact, thus it can be concluded that the formed coating layer can alleviate the harmful corrosion of the material by HF (Fig. 4d). However, it is also noted that the non-uniformity of the coating layer wrapped on the surface of the particles leads to the deteriorated Li^+transport paths, and the long-term lack of Li^+ outside will result in the increase of the Ni^{2+}/Li^+ mixed phase and inhibiting the Li^+ from migration (Fig. 4e).

To further analyze the effects of $La(PO_3)_3$ coating on the lithium-rich materials $Li_{1.2}Ni_{0.16}Mn_{0.56}Co_{0.08}O_2$, the composition of CEI film on the surface of NCM and 4% La@NCM after 100 cycles was investigated using XPS (Figs. 4f-h). In C 1s, five peaks of OCO_2, C-C, C-H, C-O and C=O for two sets of samples can be observed, where the C-C and C-H peaks are attributed to the binder PVDF, and the peaks of C-O, C=O and OCO_2 are attributed to the by-products formed during the dissolution of the electrolyte during charging and discharging. The lower peak intensities of C-O, C=O and OCO_2 of the 4% La@NCM sample compared to NCM demonstrate the effective inhibition of the electrolyte decomposition (Fig. 4f). The F spectra shown in Fig. 4g are divided into three peaks of PVDF, $Li_xPO_yF_z$ and LiF, where $Li_xPO_yF_z$ and LiF are generated by the decomposition of $LiPF_6$. The small area of the two groups of peaks in 4% La@NCM indicates that the appropriate amount of coating can effectively suppress the side reaction of the electrolyte and less $Li_xPO_yF_z$ and LiF are formed in the CEI membrane after coating. In O1s spectrum (Fig. 4h), the $ROCO_2Li$ characteristic peak of the NCM sample is clearly larger than that of the 4% La@NCM. Based on the above XPS results, it can be concluded that $La(PO_3)_3$ coating of Li-rich materials can enhance the stability of the interface to a certain extent by alleviating the corrosion of the electrode and inhibiting the decomposition of the electrolyte.

In conclusion, the Li-rich cathode materials with $La(PO_3)_3$ coating were prepared successfully by co-precipitation method. The appropriate amount of $La(PO_3)_3$ coating can improve the physical and chemical properties of cathode materials by reacting with the residual lithium on the cathode material surface. The structure can

be well stabilized by preventing the cathode materials from corrosion during long-term cycling and the oxygen loss can be reduced. The discharge specific capacity of Li-rich manganese-based cathode materials with 4% $La(PO_3)_3$ coating at 0.1 C was retained at 214.21 mAh/g after 100 cycles, with a capacity retention rate of 94.2%. This work opens a new way to improve the electrochemical performance and structural stability of lithium-rich manganese-based cathode materials.

Declaration of competing interest

The authors declare that they have no known competing financial interests or personal relationships that could have appeared to influence the work reported in this paper.

Acknowledgments

This work is supported by the Fundamental Research Funds for the Central Universities (No. 2021JCCXJD01), Key R&D and transformation projects in Qinghai Province (No. 2021-HZ-808) and Hebei Province (No. 21314401D).

Supplementary materials

Supplementary material associated with this article can be found, in the online version, at doi:10.1016/j.cclet.2022.107793.

References

[1] J.X. Meng, L.S. Xu, Q.X. Ma, et al., Adv. Funct. Mater. 32 (2022) 2113013.
[2] J.J. Zhao, Y. Xu, J. Chen, et al., Dalton Trans. 50 (2021) 9858–9870.
[3] P.F. Wu, B.Y. Shi, H.B. Tu, et al., J. Adv. Ceram. 10 (2021) 1129–1139.
[4] Y. Kim, H. Park, K. Shin, et al., Adv. Energy. Mater. 1 (2021) 2101112.
[5] X. Liu, X. Zhou, Q. Liu, et al., Adv. Mater. 34 (2022) 2107326.
[6] J.X. Hou, L. Wang, X.N. Feng, et al., Energy. Environ. Mater. 6 (2023) e12297.
[7] S.X. Yan, S.H. Luo, L. Yang, et al., J. Adv. Ceram. 11 (2022) 158–171.
[8] P.F. Wang, Ya. You, Y.X. Yin, et al., Adv. Energy Mater. 8 (2018) 1701912.
[9] E.M. Erickson, H. Sclar, F. Schipper, et al., Adv. Energy. Mater. 7 (2017) 1700708.
[10] F. Ning, B. Li, J. Song, et al., Nat. Commun. 11 (2020) 1–12.
[11] J. Lee, Q. Zhang, J. Kim, et al., Adv. Energy. Mater. 10 (2020) 1902231.
[12] J. Hong, W.E. Gent, P. Xiao, et al., Nat. Mater. 18 (2019) 256–265.
[13] G. Assat, D. Foix, C. Delacourt, et al., Nat. Commun. 8 (2017) 1–12.
[14] Y. Na, X.H. Sun, A.R. Fan, S. Cai, C.M. Zheng, Chin. Chem. Lett. 32 (2021) 973–982.
[15] Z.Y. Kou, Y. Lu, C. Miao, et al., Rare Met. 40 (2021) 3175–3184.
[16] G.T. Xiang, J.M. Yin, X.X. Zhang, P.Y. Hou, X.J. Xu, Chin. Chem. Lett. 32 (2021) 2169–2173.
[17] X.M. Deng, R. Zhang, K. Zhou, et al., Energy. Environ. Mater. (2022), doi:10.1002/eem2.12331.
[18] S.L. Cui, Y.Y. Wang, S. Liu, G.R. Li, X.P. Gao, Electrochim. Acta 328 (2019) 135109.
[19] Y. Xia, J.M. Zheng, C.M. Wang, M. Gu, Nano Energy 49 (2018) 434–452.
[20] W. Yang, C.J. Bai, W. Xiang, et al., ACS Appl. Mater. Interfaces 13 (2021) 54997–55006.
[21] Y.Y. Wang, Z.X. Zhao, J. Zhong, et al., Energy Environ. Mater. 5 (2022) 969–976.
[22] J. Sun, C. Sheng, X. Cao, et al., Adv. Funct. Mater. 32 (2022) 2110295.
[23] L. Zhou, H. Wu, M. Tian, et al., RSC Adv. 6 (2016) 69790–69797.
[24] D.M. Li, B. Zhang, X. Ou, et al., Chin. Chem. Lett. 32 (2021) 2333–2337.
[25] J. Zhao, M. Zhou, J. Chen, et al., Chem. Eng. J. 425 (2021) 131630.
[26] Y. Kim, H. Park, J.H. Warner, et al., ACS Energy Lett. 6 (2021) 941–948.
[27] K. Yuan, T.Z. Tu, C. Shen, et al., J. Adv. Ceram. 11 (2022) 882–892.
[28] B. Xiang, W.L. An, J.J. Fu, et al., Rare Met. 40 (2021) 383–392.
[29] S. Kim, W. Cho, X. Zhang, Y. Oshima, J.W. Choi, Nat. Commun. 7 (2016) 1–8.
[30] J.P. Cho, T.J. Kim, B. Park, J. Electrochem. Soc. 149 (2002) A288–A292.
[31] B. Liu, D. Wang, M. Avdeev, et al., ACS Sustain. Chem. Eng. 8 (2020) 948–957.
[32] C.F. Yang, X.S. Zhang, M.Y. Huang, et al., ACS Appl. Mater. Interfaces 9 (2017) 12408–12415.
[33] M.M. Zhou, J.J. Zhao, S.T. Qiu, et al., Int. J Electrochem. Sci. 15 (2020) 10759–10771.
[34] J. Kang, B. Han, A.C.S. Appl, Mater. Interfaces 7 (2015) 11599–11603.
[35] R.B. Yu, Y.B. Lin, Z.G. Huang, Electrochim. Acta 173 (2015) 515–522.
[36] F. Wu, Z. Wang, Y. Su, N. Yan, L. Bao, S. Chen, J. Power Sources 247 (2014) 20–25.
[37] M. Jiang, D.L. Danilov, R.A. Eichel, P.H. Notten, Adv. Energy Mater. 11 (2021) 2103005.
[38] S. Zhao, B. Sun, K. Yan, et al., ACS Appl. Mater. Interfaces 10 (2018) 33260–33268.
[39] X. Liu, T. Huang, A. Yu, Electrochim. Acta 163 (2015) 82–92.
[40] C. Zhu, J. Chen, S. Liu, et al., J. Mater. Sci. 53 (2017) 5242–5254.
[41] D. Wang, X.Y. Wang, X.K. Yang, et al., J. Power Sources 293 (2015) 89–94.
[42] Z. Feng, R. Rajagopalan, D. Sun, et al., Chem. Eng. J. 382 (2020) 122959.
[43] Z. Chen, G.T. Kim, Y. Guang, et al., J. Power Sources 402 (2018) 263–271.
[44] G.R. Hu, X.R. Deng, Z.D. Peng, K. Du, Electrochim. Acta 53 (2008) 2567–2573.
[45] Y.Z. Wang, L. Wang, X.W. Guo, et al., ACS Appl. Mater. Interfaces 12 (2020) 8306–8315.
[46] Z. Chen, J. Meng, Y. Wang, et al., Electrochim. Acta 378 (2021) 138138.
[47] D.T. Nguyen, J. Kang, K.M. Nam, Y. Paik, S.W. Song, J. Power Sources 303 (2016) 150–158.
[48] W. He, Q.S. Xie, J. Lin, et al., Rare Met. (2022) 1–21.
[49] Y. Liao, J. Li, B. Deng, et al., Energy Technol. Ger. 8 (2020) 1901133.